PAPER • OPEN ACCESS

Highly programmable 4D printed multi-shape gradient metamaterials and multifunctional devices

To cite this article: Chunli Yang *et al* 2025 *Int. J. Extrem. Manuf.* **7** 055504

View the article online for updates and enhancements.

Highly programmable 4D printed multi-shape gradient metamaterials and multifunctional devices

Chunli Yang[1,§], Xiaozhou Xin[2,§], Wenjun Zhao[2], Cheng Lin[1,4,*], Liwu Liu[2], Yanju Liu[2,3,*] and Jinsong Leng[1]

[1] Centre for Composite Materials and Structures, Harbin Institute of Technology, Harbin 150080, People's Republic of China
[2] Department of Astronautical Science and Mechanics, Harbin Institute of Technology, Harbin 150001, People's Republic of China
[3] Suzhou Research Institute, Suzhou Research Institute, Harbin Institute of Technology, Su Zhou 215100, People's Republic of China
[4] Guangzhou Institute of Future Additive Manufacturing, Guangzhou 510360, People's Republic of China

E-mail: lincheng@hit.edu.cn and yj_liu@hit.edu.cn

CrossMark

Abstract

Metamaterials, owing to their exceptional physical characteristics that are absent in natural materials, have emerged as a crucial constituent of intelligent devices and systems. However, there are still significant challenges that necessitate immediate attention, as they have considerably constrained the applicability of metamaterials, including fixed mechanical properties post-fabrication and restricted design freedom. Here, thermo-responsive, photo-responsive, electro-responsive, and magneto-responsive shape memory polymer nano-composites were developed, and shape memory gradient metamaterials were fabricated using multi-material 4D printing technology. The correlation mechanism between the design parameters and the mechanical properties of multi-responsive gradient metamaterials was systematically analyzed, and the highly designable and programmable configuration and mechanical properties of the gradient metamaterials were realized. More importantly, 4D printed multi-responsive shape memory polymer gradient metamaterials can be programmed in situ without additional infrastructure for multi-functional mechanical functions, paving the way for the realization of multiple functions of a single structure. Based on the multi-responsive gradient metamaterials, 4D printed digital pixel metamaterial intelligent information carriers were fabricated, featuring customizable encryption and decryption protocols, exceptional scalability, and reusability. Additionally, 4D printed gradient metamaterial logic gate electronic devices were developed, which were anticipated to contribute to the development of smart, adaptable robotic systems that combine sensing, actuation, and decision-making capabilities.

Int. J. Extrem. Manuf. **7** (2025) 055504

Highly programmable 4D printed multi-shape gradient metamaterials...
Yang C et al.

Supplementary material for this article is available online

Keywords: shape memory polymer nanocomposites, 4D printing,
multiple shape memory effects, bio-inspired metamaterials, multi-functionality

1. Introduction

Metamaterials are a category of functional materials formed by deliberately designed microstructural units arranged according to specific laws[1–5]. Due to the extraordinary physical characteristics that are absent in natural materials, metamaterials show significant potential for applications in flexible electronics, aerospace, and biomedicine[6–9]. Currently, however, metamaterials are mostly homogeneous periodic structures of a single material, and their configurations and mechanical properties are limited in designability. More importantly, the mechanical properties of metamaterials are fixed and lack programmable regulation ability, which leads to the serious limitation of their application scope[10–12]. Thus, the development of multi-material, gradient-structured, programmable metamaterials is of great significance to realize the high designability of their properties and configurations and to broaden the application scenarios.

Smart materials, such as shape memory polymers (SMPs), offer the possibility of post-preparation programming of metamaterials, breaking through the limitation that the mechanical properties and geometric configuration of metamaterials cannot be changed once they are prepared[13–16]. As a class of stimuli-responsive smart materials, SMPs can be programmed to temporary shapes (TS) and return to predefined initial shapes (IS) under external stimuli such as heat, light, electricity, and magnetism[17–19]. Usually, SMPs are single stimulus-responsive and only have a single temporary shape, which limits their tunable domain of structural properties and makes it difficult to meet the current increasing demand for multifunctionality and intelligence.

To address this problem, multi-shape SMPs with multiple transition temperatures were developed, which can memorize more than two temporary shapes[20–22]. Multi-shape SMPs can be achieved by broadening the phase transition temperature or multiphase design, integrating phases with discrete transition temperature into a single SMP. However, to ensure the stability and reliability of temporary shapes, a significant separation of multiple transition temperatures in the SMP is required, which severely limits the application scenarios of multi-shape SMPs, such as biomedical and wearable electronic devices. Besides, synthesizing SMPs with multiple separated phase transition temperatures becomes extremely challenging as the number of separated phase transitions rises, which is not approachable for scale production with practical applications. Therefore, it is urgent to develop a method for manufacturing multi-shape SMPs, which is facile to implement, economical, fast and accurate.

Here, to realize the high programmability, tunability and versatility of metamaterials, multi-responsive, multi-shape

shape memory nano-composites (SMCs) gradient metamaterials were prepared in a straightforward and cost-effective way using multi-material 4D printing technology, demonstrating potential applications in intelligent information carriers and intelligent flexible robotic system (Figure 1). SMCs featuring different stimulus responses (thermo-responsive, photo-responsive, electro-responsive, and magneto-responsive) were integrated into a metamaterial structure by multi-material 4D printing, and multiple shape memory effects as well as spatiotemporally controllable selective actuation were realized by applying specific stimuli. A diversified design of metamaterial structures was conducted from various perspectives, including ligaments, nodes, gradient materials, and gradient architectures, to achieve enhanced diversification and tunability of mechanical properties. It is worth noting that the introduction of thermally, optically, electrically, and magnetically responsive materials, combined with gradient structure design, endowed metamaterials with diverse, tunable, and programmable configurations and mechanical properties. This enhanced the design freedom of metamaterials and broadened the tunable range of mechanical properties. Based on multi-responsive gradient metamaterials, combined with binary language and Morse code, encodable digitized pixel metamaterial intelligent encrypted carriers were designed with self-assembly, scalability, and encrypted transmission of massive information. Variable stiffness logic electronic devices, developed with multi-shape gradient metamaterials, allowed devices to switch between rigidity and flexibility, enabling precise control of digital signals and circuits, which was expected to smooth the path for multi-environment soft robots and interactive machines.

2. Results and discussions

2.1. Preparation and characterization of 4D printed SMCs

By employing multi-responsive SMCs and multi-material 4D printing technology, gradient metamaterials were fabricated. Multi-material 4D printing allowed for the precise preparation of complex structured metamaterials with programmable structures and properties, killing two birds with one stone. 4D printing adds an additional time dimension to 3D printing, allowing 3D printed structures to dynamically change shape or properties over time after preparation. Combining 3D printing with intelligent programmable material (e.g. SMCs) can achieve 4D printing. 4D printing inherits the advantages of 3D printing in terms of personalization of manufactured structures, fast preparation speeds, and high processing accuracy, and adds the ability
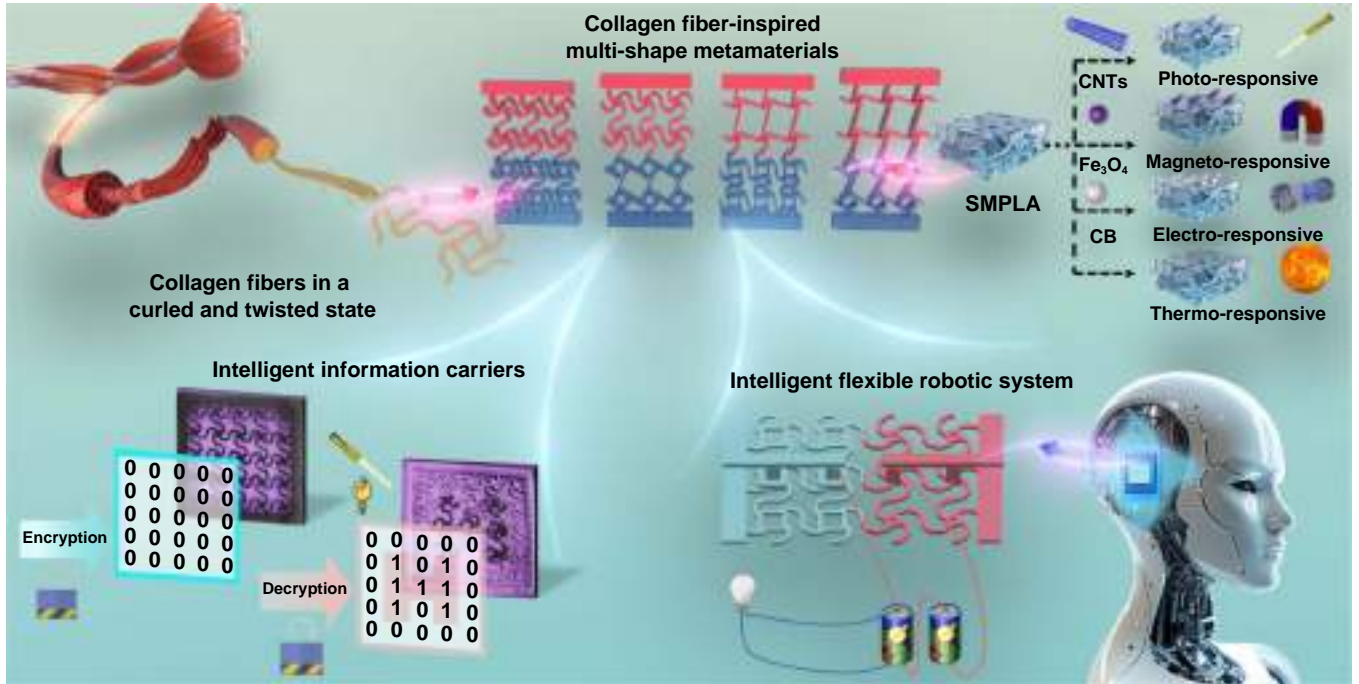
Figure 1. The design principle and applications of 4D printed multi-shape gradient metamaterials.

for structures to be dynamically transformable in time and space[23–27].

Multi-responsive 4D printing SMCs were fabricated by introducing functional components to SMP matrix, and multi-shape metamaterials were prepared by combining different stimuli-responsive 4D printing SMCs, which endowed the structures with highly programmable properties and selective precision actuation. Multi-responsive 4D printing SMCs included photo-responsive, electro-responsive, magneto-responsive, and thermo-responsive shape memory composites. The shape transformation ability of 4D printing SMCs was attributed to the combination of the fixed phase and the switchable phase. The switchable phase was movable molecular chains that were reversibly activated or frozen, which determined the shape-fixing performance of SMCs. The temperature at which the switchable phase underwent a state change was defined as the shape memory transition temperature (T_{trans}) of SMCs, which was also equivalent to the glass transition temperature (T_g) of SMCs. The fixed phase consisted of physical crosslinking points formed by polymer chain entanglements or chemical crosslinking points formed by covalent bonds, which enabled SMCs to remember the initial shapes and ensured the shape recovery process. 4D printing photo-responsive shape memory composites (P–SMC) were prepared using shape memory polylactic acid (SMPLA) as substrate and introducing functional component carbon nanotubes (CNTs). CNTs were able to absorb light energy and convert it into heat energy, heating polymer molecular chains above the shape memory transition temperature, and promoting the shape memory process. The carbon black (CB) nanoparticles and iron tetraoxide (Fe_3O_4) magnetic

nanoparticles were introduced to prepare 4D printed electro-responsive shape memory composites (E–SMC) and magneto-responsive shape memory composites (M–SMC). When electric fields and alternating magnetic fields were applied, the polymer molecular chains were heated due to the presence of CB nanoparticles and magnetic nanoparticles, thus achieving programmable shape memory properties. The SMPLA matrix was capable of responding to thermal stimuli and was therefore notated as 4D printed thermally responsive shape memory composites (T–SMC).

Figure 2(a) illustrates the process of preparing multi-responsive SMCs 4D printing filaments by melt extrusion. These shape memory composite filaments were compatible with commercial FDM printers, enabling the high-precision fabrication of complex structures and exhibiting superior print quality (Figure S1). The crystalline phase and structural information of the four SMCs were characterized by XRD (Figure 2(b)). T–SMC showed a broad "bun peak" between 10°–25°, indicating its amorphous molecular structure. After the addition of the functional components, P–SMC, E–SMC, and M–SMC all showed a strong diffraction peak at around 16.5°, corresponding to the (200) and (110) crystal planes of SMPLA, possibly because the functional components improved the crystallinity of the polymer matrix. Compared with T–SMC, P–SMC exhibited an additional diffraction peak at approximately 25.5°, which proved the successful loading of CNTs. With the addition of CB, the E–SMC showed a small and broad peak at approximately 26.0°, corresponding to the characteristic peak of the (002) crystal plane of CB. In the XRD pattern of M–SMC, three significant characteristic peaks appeared at $2\theta \approx 29.8°$, $35.4°$, and $43°$,

Int. J. Extrem. Manuf. **7** (2025) 055504

Highly programmable 4D printed multi-shape gradient metamaterials...
Yang C et al.

corresponding to the (220), (311), and (400) crystal planes of Fe_3O_4 nanoparticles. In addition, the thermal analysis results showed that the introduction of functional fillers slightly increased the glass transition temperatures of the SMCs. The transition temperatures of T–SMC, M–SMC, E–SMC, and P–SMC were 59.4 °C, 63.53 °C, 63.74 °C and 62.37 °C, respectively (Figure 2(c)), which may be due to the interface interaction between the functional fillers and the polymer matrix, and the functional fillers inhibiting the migration of polymer molecular chains. In addition, the cold crystallization peak of SMPLA shifted to lower temperatures due to the incorporation of functional fillers, indicating that the introduction of functional fillers promoted the cold crystallization of SMPLA. On the contrary, with the addition of functional fillers, the melting peak of the three SMCs shifted to higher temperatures, but all remained around 170 °C. Figure 2(d) illustrates the relationship between the storage modulus of SMCs and temperature. The results indicated that within the glass transition range, the storage modulus of the four SMCs exhibited a sharp decline. Furthermore, the addition of functional components reduced the storage modulus of SMPLA at room temperature, enhancing the SMCs's flexibility. When the temperature exceeded 100 °C, the storage modulus of the SMCs began to increase, which was attributed to the cold crystallization of SMPLA above 100 °C, consistent with the DSC results. The morphology of the SMCs verified this phenomenon, the surface of T–SMC was flat and no second phase appeared (Figure 2(e)). Whereas, the morphology of P–SMC showed uniformly dispersed CNTs and tubular structured CNTs (with diameters between 70–180 nm) were observed (Figure 2(f)). In E–SMC, conductive CB nanoparticles were also clearly observed and uniformly dispersed in the matrix as spherical particles with diameters of 80–120 nm (Figure 2(g)). Compared with E–SMC, the nanoparticle size was larger in M–SMC, and the Fe_3O_4 nanoparticles were embedded in the matrix and tightly bound to the matrix (Figure 2(h)). The functional groups of 4D printed P–SMC, E–SMC, M–SMC and T–SMC were analyzed using FTIR spectroscopy. The four 4D printed SMCs exhibited strong –C=O absorption peaks at about 1 749 cm^{-1}, while the characteristic peaks at 2 998 cm^{-1} and 2 946 cm^{-1} were attributed to asymmetric and symmetric vibrations of –CH$_3$ (Figure S2). Furthermore, the absorption peak observed at approximately 584 cm^{-1} was ascribed to the vibration of the Fe–O bond, confirming the successful incorporation of Fe_3O_4 nanoparticles. The XPS spectra showed that the P–SMC, E–SMC, and T–SMC were all composed of C and O elements, while the M–SMC showed an additional Fe element (Figure S3). The C1s consisted of three peaks (284.3 eV, 286.7 eV, and 288.8 eV), which were attributed to C–H, C–O, and C=O chemical bonds (Figure S4(a)). The characteristic peaks of C–O (531.6 eV) and C=O (533.4 eV) in the XPS spectrum O1s were observed, and the M–SMC exhibited an additional Fe–O characteristic peak (530.8 eV) (Figure S4(b)). As shown in Figure S5, two characteristic peaks at 724.3 eV and 715.1 eV corresponded to Fe2p$_{1/2}$ and Fe2p$_{3/2}$, respectively, further confirming the presence of Fe_3O_4 nanoparticles.

2.2. Programmable stimulus responsiveness of the 4D printed SMCs

The 4D printed P–SMC was able to respond to light stimuli to realize non-contact and precise control of the shape memory process of the sample (Figures S7–S11). As shown in Figure 3(a), the lower pair of wings of the dragonfly was assigned as a folded temporary shape, and the photo-responsive programmable shape recovery properties of the 4D-printed dragonfly were explored. The left and right wings were actuated precisely and selectively, with an extremely fast recovery time (within 5 s) and a recovery rate close to 100% (Movie S1). Durability tests were conducted on dragonfly samples at 50 °C, and the shape memory performance of the samples after the tests was characterized. The results indicated that after 20 cycles, the shape recovery ratio (R_r) remained above 99% (Figures S12–S16, Movie S2). In addition, the feasibility of the 4D printed SMC as a drive hinge was analyzed (Figure 3(b)). When the 4D printed P–SMC hinges were in temporary shape, the spacecraft sail panels were in a folded state. When the light stimulus was applied, the 4D printed P–SMC hinge was actuated, enabling controlled deployment of the spacecraft sail panel. What's more, electrically responsive samples of structures such as infants were designed and prepared using 4D printing technology, demonstrating once again the excellent printability of the developed 4D printing SMCs. The infant sample was configured into a temporary shape and an electric field was applied. The Joule heat generated by the CB nanoparticles caused the temperature of the sample to rise, and the shape recovery process was successfully carried out (Figure 3(c)). Temperature monitoring by an infrared thermal imaging system showed that the 4D printed E–SMC can reach temperatures of up to 70 °C or more. The "U" shaped, four-leaf clover and villain samples also validated the excellent electrically responsive shape memory properties of the 4D printed E–SMC (Figures S17–S19). Similarly, the rapid magnetic response characteristic of M–SMC was evaluated, which can achieve a considerable deformation of 350% and quickly return to its initial shape under an alternating magnetic field (Figure S20).

In addition, the selective actuation performance of 4D printed SMCs with multiple shape memory effects was evaluated. The multi-shape dragonfly, toothless, and scorpion were prepared by 4D printing using two different responsive materials, P–SMC (black part) and T–SMC (green part) (Figures 3(d)–(f)). A temporary shape was obtained by programming the 4D printed multi-shape toothless to a folded wing state (Figure 3(d)). Upon the application of light, the P–SMC region was selectively actuated to revert to its initial shape, while the T–SMC region remained unchanged, so the toothless acquired an additional temporary shape. During this process, infrared thermograms showed that only the temperature of the P–SMC region increased significantly, while the temperature of another region remained unchanged. When thermal stimulation was applied, the T–SMC region returned to the initial shape, realizing multiple shape memory effects and spatiotemporally selective controllable actuation.
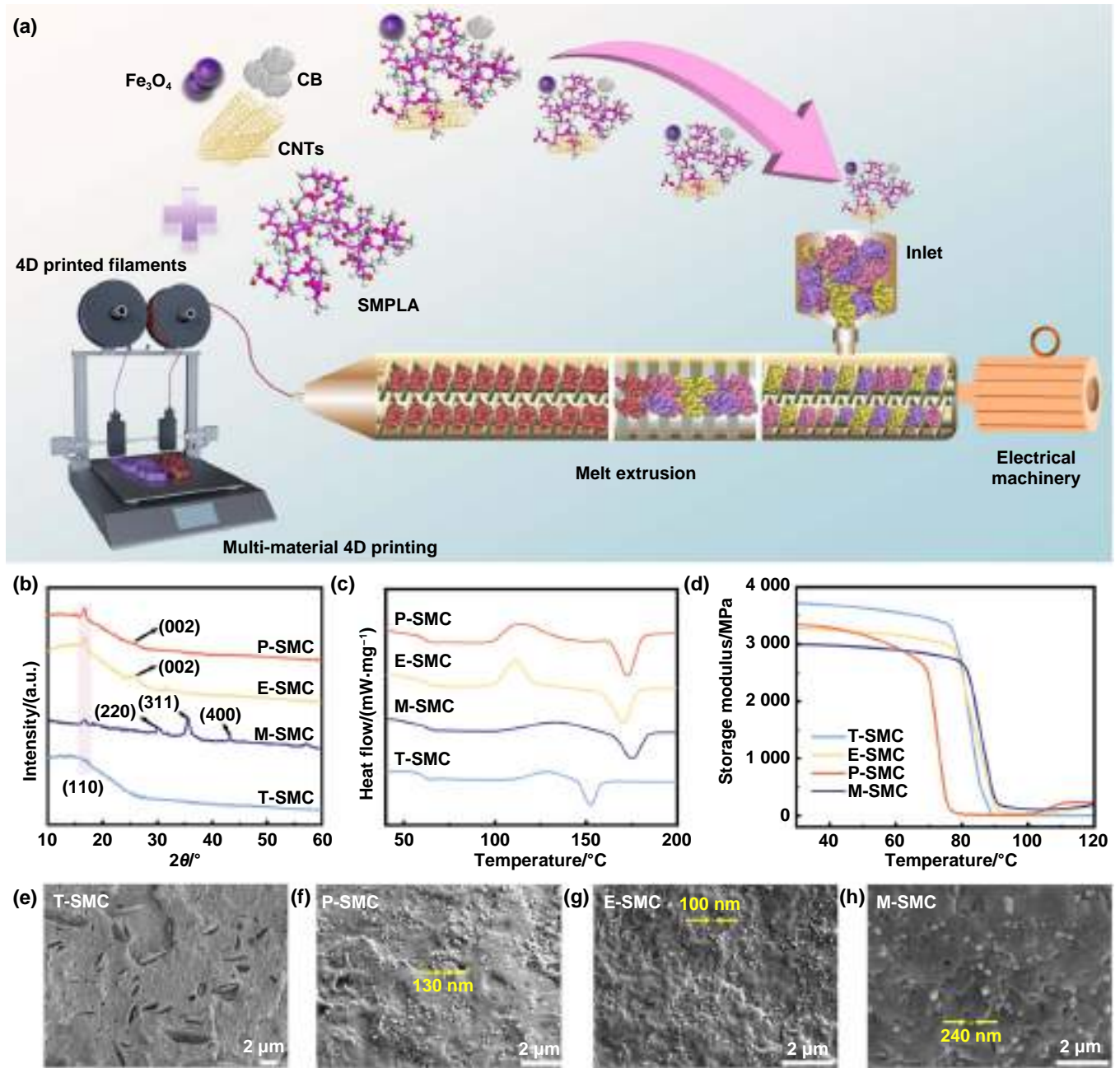
Int. J. Extrem. Manuf. 7 (2025) 055504

Highly programmable 4D printed multi-shape gradient metamaterials...
Yang C et al.

Figure 2. Preparation and characterization of multi-responsive 4D printing SMCs. (a) Preparation of the shape memory composite filaments and the multi-material printing process. (b) XRD patterns. (c) DSC curves. (d) DMA curves. (e)–(h) Morphology analysis: (e) T–SMC, (f) P–SMC, (g) E–SMC, and (h) M–SMC.

Similarly, the dragonfly sample was programmed to be in a folded wing state, and the scorpion sample was programmed to be in an attacking state with both pincers raised and tail upside down (Figures 3(e) and (f)). The samples were able to acquire additional temporary shapes through photo/thermal dual stimulation and sequentially reverted to their initial shapes. The temperature monitoring of the samples indicated that the temperature was increased in the target region, while the non-target region was in a low-temperature state, which can achieve effective temperature control. Therefore, the multishape memory effect of the multi-shape 4D printed SMCs was verified and the spatio-temporal selective controllable actuation was realized. Meanwhile, in Figures S21 and S22, it was demonstrated that the 4D-printed SMCs with selective actuation properties can be employed to lift and release objects.

2.3. Highly programmable multi-shape gradient metamaterials

2.3.1. Design of four-ligament gradient metamaterials.
Gradient metamaterial structures with bionic wave-like ligaments were designed, inspired by the curled and twisted
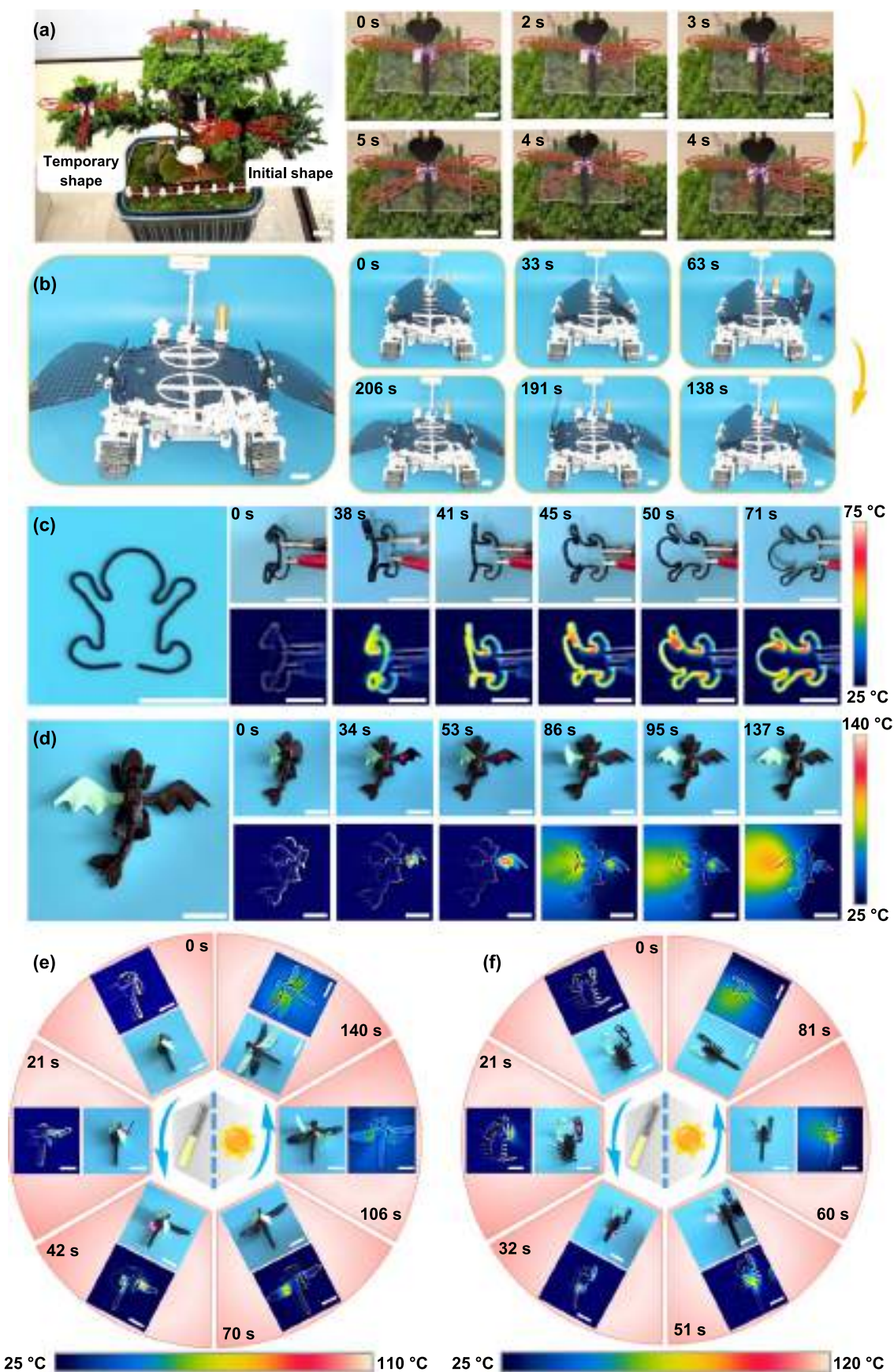
Int. J. Extrem. Manuf. **7** (2025) 055504

Highly programmable 4D printed multi-shape gradient metamaterials...
Yang C et al.

Figure 3. Programmable stimulus responsiveness of the 4D printed SMCs. (a) Photo-responsive programmable shape memory properties of the 4D printed dragonfly sample. (b) The 4D printed photo-responsive hinge structure for controllable deployment of sail panels in a spacecraft model. (c) Programmable shape memory process and temperature evolution of 4D printed electrically responsive infant sample. (d)-(f) Spatio-temporal selective shape recovery process and temperature evolution of 4D printed multi-shape samples under multiple stimuli: (d) 4D printed toothless, (e) 4D printed dragonfly, and (f) 4D printed scorpion. Scale bar = 2.5 cm.

Int. J. Extrem. Manuf. 7 (2025) 055504

Highly programmable 4D printed multi-shape gradient metamaterials...
Yang C et al.

collagen fibers in biological tissues[28, 29]. The metamaterial cell consisted of wave-like ligaments and nodes with rotational symmetry properties. Gradient metamaterials were designed in terms of the number of ligaments, ligament configuration, and node configuration. To achieve selective and precise actuation, the bionic metamaterials were prepared using multi-responsive 4D printed SMCs, where four-ligament metamaterials were prepared by 4D printed P–SMC and M–SMC. The structural design of the four-ligament metamaterial is shown in Figure 4, and the main geometrical parameters include d/n, w/n, and angle θ (Figure 4(a)). The photo/magnetic dual-responsive metamaterial with a ligament angle of 100 and a square node edge length of 3 mm (n = 3) was denoted as P100n3–M100n3. Metamaterials with ligament angles of 120°, 140°, and 160° were also designed, noted as P120n3–M120n3, P140n3–M140n3, and P160n3–M160n3, respectively (Figure 4(b)). In terms of the number of ligament variations, four-ligament metamaterials and six-ligament metamaterials were designed. In terms of ligament configuration variations, gradient metamaterials were designed, including gradient metamaterials with ligament angles of 100° and 120° (P100n3–M120n3), gradient metamaterials with ligament angles of 120° and 140° (P120n3–M140n3), etc. (Figure 4(c)). In terms of node configuration variations, the metamaterials P160n0–M160n0, P160n3–160n6, P160n6–M160n6, etc., were designed with square node edges of 0 mm (point nodes), 3 mm, and 6 mm (Figure 4(d)). In addition, nested metamaterials (NM) with nested multilevel node structures were designed, in which metamaterial unit structures were nested in pristine metamaterial nodes, with the structural parameters including θ', θ, n', n, d'/d, d/n, w/n. According to the preparation materials and ligament angle, the NMs were denoted as NM–P100n6–M100n6, NM–P120n6–M120n6, etc. (Figure 4(e)).

2.3.2. Selective actuation mechanism of multi-shape gradient metamaterials.

The photo/magnetic dual-responsive four-ligament metamaterials with wavy ligaments were prepared by multi-material 4D printing technology. The photo-responsive region was denoted by P, the magneto-responsive region was denoted by M, and the initial and temporary shapes were denoted as IS and TS, respectively. The metamaterial where both photo-responsive and magneto-responsive regions were of initial shape was called P IS–M IS, and if both photo-responsive and magneto-responsive regions were of temporary shape, it was called P TS–M TS. P TS–M IS and P IS–M TS represented metamaterials with photo-responsive region in temporary shape and magneto-responsive region in temporary shape, respectively. The 4D printed metamaterial enabled 3 temporary shapes (P TS–M IS, P IS–M TS, P TS–M TS), and 2 (P TS–M IS, P IS–M TS) of them were additionally obtained by combining the programmable shape memory properties with the multishape properties.

At room temperature, the molecular chains in SMCs were freely arranged with the highest entropy. When light was applied, CNTs in the photo-responsive metamaterial region absorbed light energy and converted it to thermal energy (photothermal effect), which was then transferred to the surrounding molecular chains. After the temperature of the molecular chains was increased above T_g, the switchable phase was activated, the mobility of the molecular chains increased and was readily assigned a shape under external tensile loading. At this point, the molecular chains of the switchable phase oriented along the loading direction and became frozen (fixing the temporary shape), thereby reducing the system's entropy. The macroscopic manifestation was that the photo-responsive metamaterial ligaments were deformed into straight temporary shapes. In contrast, the magneto-responsive metamaterial region was unable to respond to light stimulation and the molecular chains remained frozen. The initial shape of ligaments remained unchanged even with external tensile loads. As a result, the photo-responsive region was in a temporary shape and the magneto-responsive region was in an initial shape, realizing a selectively controllable actuation (P TS–M IS). Similarly, when an alternating magnetic field was applied, magnetic nanoparticles produced high hysteresis. The molecular chains were heated and mobility was enhanced. The magneto-responsive region was easily assigned to a temporary shape, while the photo-responsive region remained in its initial shape, and another additional temporary shape of the metamaterial was thus produced (P IS–M TS). If both light and magnetic stimuli were applied simultaneously, the ligaments in both regions of the 4D printed metamaterial were deformed into a straightened temporary shape (P TS–M TS) (Figure 5(a)).

2.3.3. Highly programmable mechanical properties of metamaterials.

The multi-shape characteristics of metamaterials endowed them with the ability to incorporate additional temporary shapes, facilitating highly programmable mechanical performance (Figures 5(b)–(e)). The four states of metamaterials exhibited different mechanical properties, facilitating the realization of multiple uses of a single structure/device. P IS–M IS had a wavy ligament structure, and the ligament curvature decreased gradually at the beginning of stretching, with the deformation of the metamaterial dominated by bending. As stretching proceeded, the metamaterial ligaments gradually approached the limit of bending deformation and the metamaterial deformation transformed to tensile dominance. The elongation at break of the metamaterials was higher due to the bending-dominated deformation phase as a buffer, while the tensile strength of the metamaterials was at a lower level. In contrast, the ligaments of both photo-responsive and magneto-responsive metamaterials were almost linear after they were programmed (P TS–M TS). The deformation of metamaterial was dominated by the tension only, and the elongation at break decreased. The tensile strength showed significant enhancement due to the prominently increased structural effective stiffness of the straight ligament metamaterials. P TS–M IS and P IS–M TS were combinations of flexural and straight ligaments, so their mechanical properties were intermediate between those of P IS–M IS and P
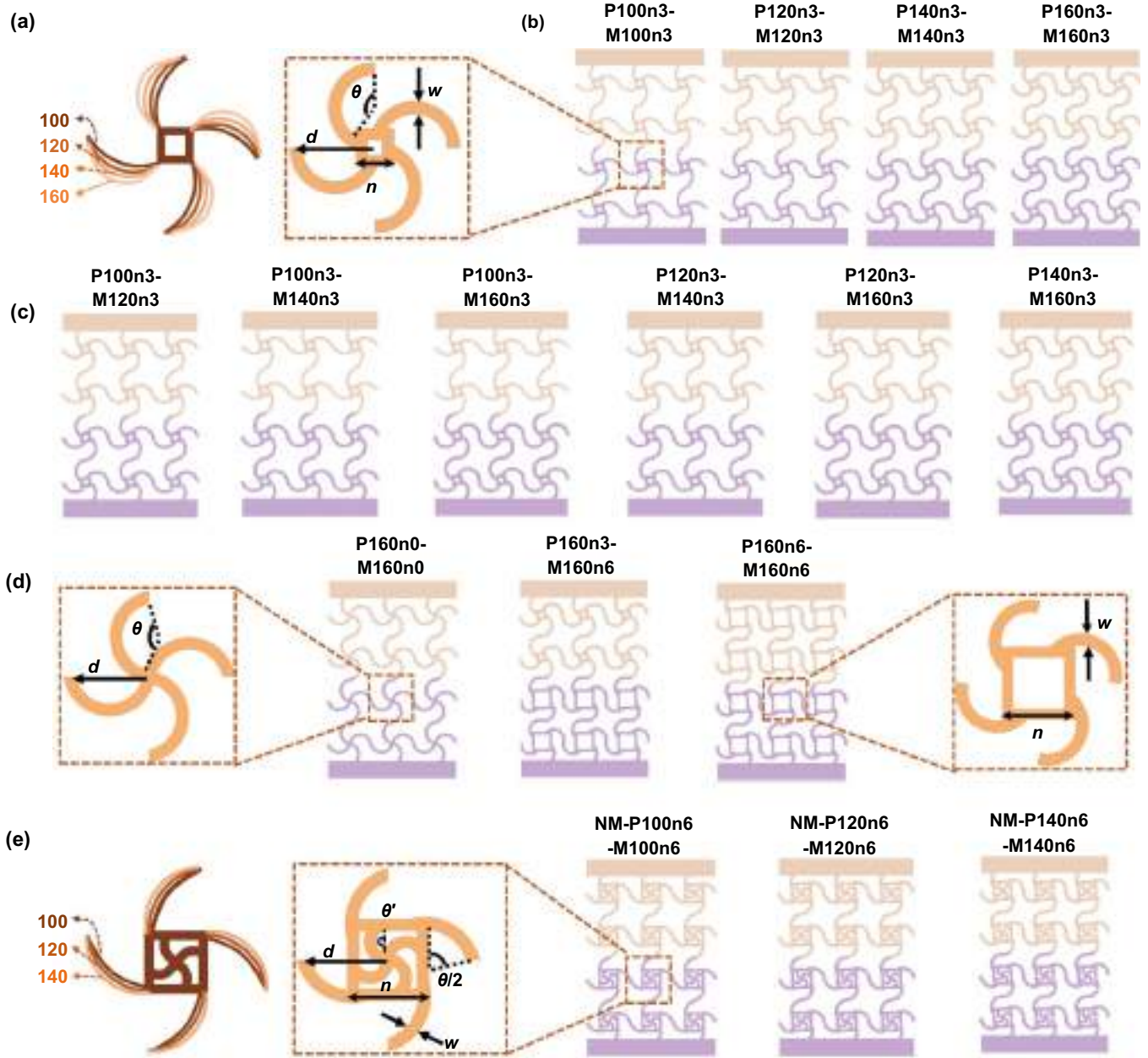
Int. J. Extrem. Manuf. 7 (2025) 055504

Highly programmable 4D printed multi-shape gradient metamaterials...
Yang C et al.

Figure 4. Structural design of four-ligament gradient metamaterials. (a) Design parameters of the metamaterial cell. (b) Design of metamaterials with different ligament configurations. (c) Structural design of gradient metamaterials with variable ligaments. (d) Structural design of gradient metamaterials with variable nodes. (e) Structural design of nested multilevel metamaterials.

TS–M TS. In general, the tensile strength of P TS–M TS was higher than that of P TS–M IS, whereas the elongation at break exhibited the opposite trend. Consequently, selective programming not only enhanced the tensile strength of the metamaterials but also broadened the application range by balancing the difference between strength and toughness.

The effect of ligament configuration on the mechanical properties of metamaterials was investigated (Figure 5(b)). When the ligament angles of the photo-responsive and magneto-responsive regions were identical, the effective stiffness of the metamaterial decreased as the ligament angle increased. As the ligament angle increased, the central angle of the metamaterial ligaments reduced, leading to a decrease in the bending-dominated deformation region, thereby increasing the effective stiffness of the metamaterial. Thus, overall, the tensile strength of the metamaterials in the initial shape decreased gradually with the increase of the ligament angle. The tensile strength of P100n3 IS–M100n3 IS was 420 kPa, while the tensile strength of P160n3 IS–M160n3 IS decreased to 210 kPa. In addition, as the ligament angle increased, the greater the difference between the tensile strength of the initial and temporary shapes of the metamaterial. The tensile strengths of the temporary shapes of P100n3–M100n3, P120n3–M120n3, and P160n3–M160n3 were 2.60, 3.48, and 4.43 times higher than those of their initial shapes, respectively. Therefore, the multi-shape metamaterials
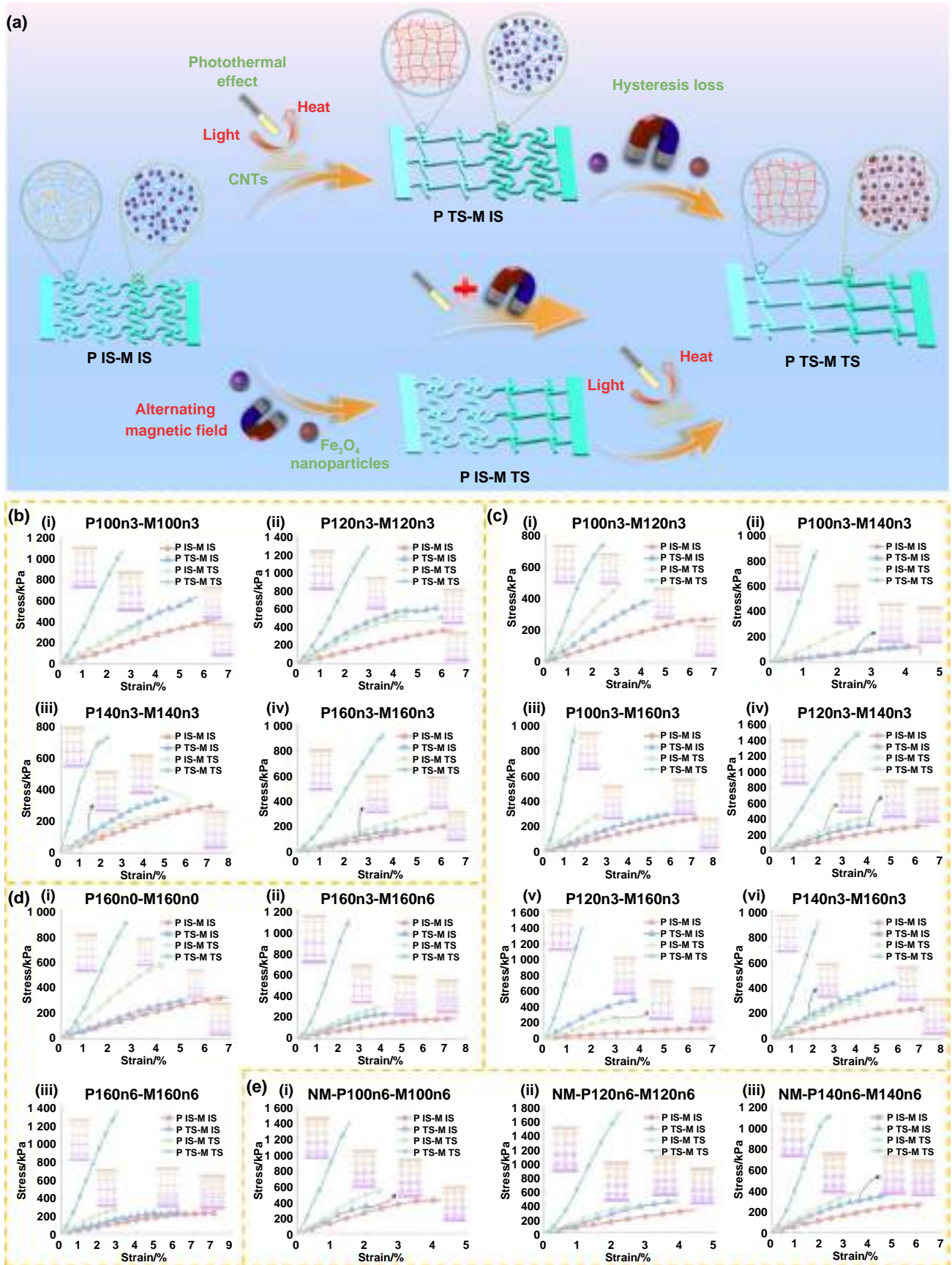
Int. J. Extrem. Manuf. 7 (2025) 055504

Highly programmable 4D printed multi-shape gradient metamaterials...
Yang C et al.

Figure 5. Highly programmable mechanical properties of metamaterials. (a) Selective actuation mechanism of multi-shape gradient metamaterials. (b)–(e) Programmable mechanical properties of four-ligament gradient metamaterials: (b) Metamaterials with different ligament configurations, (c) gradient metamaterials with various ligaments, (d) gradient metamaterials featuring variable nodes, and (e) nested multilevel gradient metamaterials.

Int. J. Extrem. Manuf. **7** (2025) 055504

Highly programmable 4D printed multi-shape gradient metamaterials...
Yang C et al.

ligament angles can be adjusted to regulate the difference of their programming mechanical properties. Large ligament angles were suitable for scenarios requiring a wide range of tensile strengths, while small ligament angles were suitable for application scenarios requiring fine tuning of tensile strengths.

Figures 5(c) and (d) analyzed how ligament configuration and gradient ligaments affect the programmed mechanical properties of metamaterials. The larger the difference in the angle of the ligaments in the two regions of the gradient metamaterial, the higher the tensile strength of P TS–M TS, and the more pronounced the difference in tensile strength between its temporary and initial shapes. In contrast, the elongation at break of the three temporary shapes was negatively correlated with the difference in ligament angles. Therefore, the angular difference of the gradient ligaments of gradient metamaterials can be adjusted to further broaden the tunable range of the mechanical properties of metamaterials. Figure 5(d) revealed the impact of node size on the mechanical properties of metamaterials. The elongation at break of the initially shaped metamaterials increased significantly with increasing node size, and the P160n6 IS–M160n6 IS exhibited the highest fracture elongation. The mechanical properties of metamaterials with nested nodes were analyzed (Figure 5(e)). Overall, the strength of the nested metamaterials was significantly increased compared to the conventional square nodes. The tensile strength of NM–P100n6 TS–M100n6 TS was increased to 1 400 kPa, and the tensile strength of NM–P120n6 TS–M120n6 TS was close to 1 800 kPa. Therefore, the nested node structure can be designed to realize the design of the tensile strength. However, there was a slight decrease in the fracture elongation of the nested metamaterials, which was attributed to the introduction of the internal nested structure at the nodes, resulting in a significant increase in ligament stiffness. In addition, part of the ligaments was occupied by nodes, and the toughness of the overall structure decreased. The secondary nested structure was demonstrated here, and future research on the multilevel nested structures can be carried out to deeply analyze their effect on the mechanical properties. Figure S25 illustrates the deformation behavior of gradient metamaterials under different loading conditions. During the tensile process, the deformation primarily concentrated on the ligaments, while the square nodes exhibited rotational deformation. Throughout the deformation process, the maximum principal strain was predominantly localized at the inflection points of the ligaments, which may be attributable to stress concentration.

2.3.4. Design of six-ligament gradient metamaterials.

In addition, six-ligament metamaterials with different structural parameters were designed to investigate the effects of ligament and node configuration on their mechanical properties. The cell structure of the six-ligament metamaterial is shown in Figure 6(a), and the design parameters mainly include d/n, w/n, t/n, and θ. Six-ligament metamaterials were prepared by 4D printing E–SMC and T–SMC. A multi-shape gradient metamaterial was designed with a ligament angle of 100° in the electro-responsive region, a ligament angle of 140° in the

thermo-responsive region, and a square node edge length of 3 mm, denoted as E100n3–T140n3 (Figure 6(b)). Similarly, metamaterials such as E120n3–T140n3 and E120n3–T160n3 were also designed. In terms of node size variation, metamaterials with square node side lengths of 0 mm, 3 mm, and 4 mm were designed, including E160n0–T160n4, E160n3–T160n4, etc. (Figure 6(c)). Six-ligament and four-ligament gradient metamaterials exhibited similar programmable mechanical properties. By selectively and controllably actuating the multi-shape metamaterials, the metamaterials can be freely switched among the four shapes, realizing highly programmable mechanical properties with high design freedom (Figure 6(d) and (e)). When both the electro- and thermo-responsive regions of the gradient metamaterial were in the initial shape (E IS–T IS), the wavy ligament deformed into a mixed mode of bending and tensile dominance upon being subjected to tensile loading. The structural effective stiffness and tensile strength of the metamaterials were at a lower level, while the elongation at break was at a higher level. The ligaments were straightened and the deformation mode was tensile dominant when both the electro- and thermo-responsive regions of the metamaterial were in temporary shape (E TS–T TS). The E TS–T TS metamaterials had higher tensile strength but lower elongation at break. The mechanical properties of metamaterials with mixed programming deformation (E IS–T TS and E TS–T IS) were between E IS–T IS and E TS–T TS. In general, the variability in the mechanical properties of the four programmed shapes of the six-ligament metamaterials was significantly reduced compared to the four-ligament metamaterials. The tensile strength of the six-ligament metamaterial in the E IS–T IS state was conspicuously greater than that of the four-ligament metamaterial. This may be ascribed to the increased number of ligaments that can withstand greater tensile loads.

The influence of ligament angle on the mechanical behavior of gradient metamaterials was investigated (Figure 6(d)). Elongation at break and tensile strength of E IS–T IS increased with the ligament angle difference (E120n3–T140n3 < E100n3–T140n3, E140n3–T160n3 < E120n3–T160n3, E120n3–T140n3 < E120n3–T160n3, E140n3–T160n3 < E100n3–T140n3). For instance, the tensile strength of E120n3 TS–T140n3 TS exceeded 1 600 kPa, while E120n3 TS–T160n3 IS and E120n3 IS–T160n3 IS exhibited excellent toughness, elongation at break was greater than 9.0%. In addition, the impact of node size on the mechanical characteristics of metamaterials was investigated (Figure 6(e)). For six-ligament metamaterials, the decrease in node size contributed to the increase in tensile strength. This may be due to the fact that the aggregation of six-ligament metamaterial ligaments at point nodes led to a higher surface coverage in localized areas, which was higher than that of square nodes, resulting in elevated strength. E160n0 TS–T160n0 TS had the highest tensile strength, approximating 1 200 kPa, whereas the elongation at break of E160n0 IS–T160n0 IS was the minimal. The tensile strength of the metamaterial decreased as the node size increased, whereas the elongation at break of the metamaterial at the initial shape was essentially positively correlated with the node size. Figure 6(f) demonstrates the P120n3–M120n3 and E120n3–T140n3 multi-responsive 4D
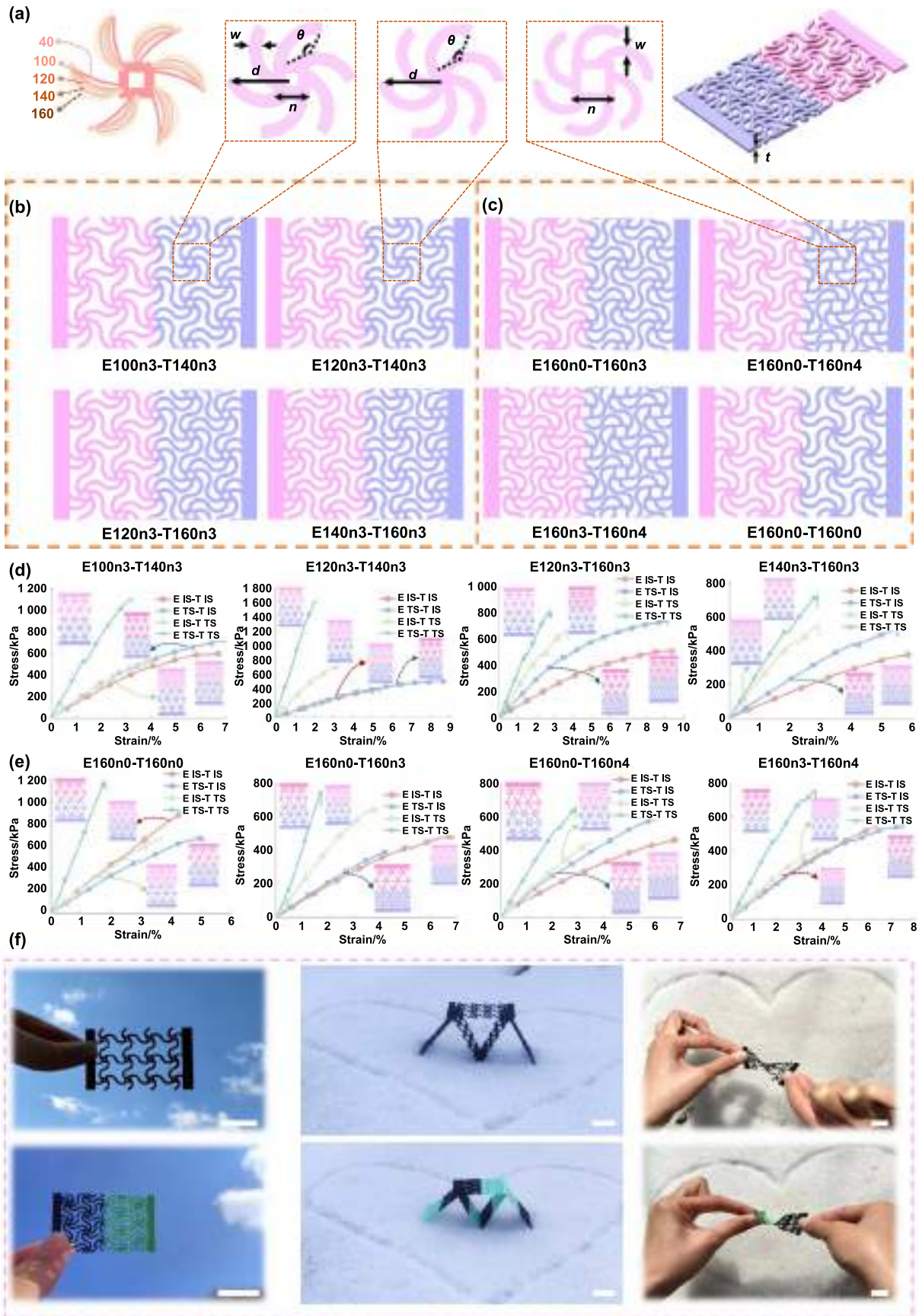
Int. J. Extrem. Manuf. **7** (2025) 055504

Highly programmable 4D printed multi-shape gradient metamaterials...
Yang C et al.

Figure 6. Structural design of six-ligament gradient metamaterials. (a) Design parameters of the metamaterial cell. (b) Structural design of six-ligament gradient metamaterial with variable ligament configuration. (c) Structural design of six-ligament gradient metamaterial with variable node configuration. (d) and (e) Programmable mechanical properties of six-ligament gradient metamaterials. (f) Demonstration of 4D printed metamaterials and their flexibility. Scale bar = 2 cm.

Int. J. Extrem. Manuf. **7** (2025) 055504

Highly programmable 4D printed multi-shape gradient metamaterials...
Yang C et al.

printed gradient metamaterials. After printing, the node and ligament structures of the metamaterials can be accurately reproduced with smooth and flat surfaces. Due to the transition from bending-dominated to tension-dominated behavior during the deformation process, the multi-responsive gradient metamaterials also demonstrated excellent flexibility and deformation capability even in harsh external environments, greatly broadening their practical applications. They were able to maintain a high degree of flexibility in snow at -10 °C, overcoming the inherent brittleness of the SMPLA matrix and realizing a significant improvement in performance through structural design (Figure S29).

2.4. Applications of 4D printed multi-shape metamaterials

2.4.1. Intelligent information carrier. In the era of informatization, with the booming development of the Internet of Things and 5 G wireless communication technology, information security is extremely crucial. Here, inspired by the binary language, based on 4D printed multi-responsive gradient metamaterials, encodable digital pixel metamaterial (DPM) intelligent information carriers were designed, which were characterized by reliable information transmission, high security, and facile manufacturing process. Each cell of the DPM was a pixel, and the deformed and undeformed cells were encoded in situ as programmable pixels of "1" (deformed) and "0" (undeformed). Thus the digitized pattern information of (i × j) pixels allowed for conversion to ($2^{i \times j}$) possible mechanical information[30]. With 160n3–160n3 metamaterial as the DPM intelligent information carrier (Figure 7(a)), each carrier unit was composed of 5 pixel × 5 pixel with different stimulus-response characteristics, and multiple metamaterial carrier units constituted a metamaterial information carrier sequence. In the process of information transmission, the stimulus-response signal was used as a symbolic language, and 4D printed DPMs responded to different stimuli to enable the encryption and decryption of information. The non-actuated metamaterial was in an encrypted state without any information being displayed. Once the metamaterial carrier was actuated by the predefined stimulation program, the encrypted text "HIT" (abbreviation of Harbin Institute of Technology) was gradually displayed. The information to be transmitted was programmed in situ as a binary sequence consisting of 0 and 1, and the encrypted information was digitized to improve the transmission efficiency and accuracy of the decrypted information (Figure 7(a)). More interestingly, the DPM information carrier can not only encrypt text information, but also provide a facile way to transmit complex information. As shown in Figure 7(b), by selectively actuating the DPM information carrier, expressions such as "smiley face", "angry face", and "sad face" were obtained. Additionally, the feasibility of decrypting the 4D printed DPM through the electrostimulation program was verified (Figure 7(c)). The 160n0–160n3 gradient metamaterial of the six ligaments was used as the information carrier, and after decryption by electrical stimulation, the "4DP" information was displayed.

In addition, programmable Morse code intelligent information carriers were developed by combining 4D printed DMP,

multi-stimuli actuating method and Morse code. Morse code is an internationally recognized means of encrypting communications through the expression of dots (".") and dash ("–") to realize the encrypted transmission of information. As shown in Figure 7(d), a multishape 160n3–160n3 DMP information carrier with 17 pixel × 5 pixel was fabricated from P–SMC and M–SMC by 4D printing technology. When the DPM information carrier was exposed to light, the photo–responsive pixels were deformed while the magneto–responsive pixels remained unchanged. The deformed pixels were noted as "–" and the undeformed pixels were noted as ".", presenting a Morse code of "–.–.–.–.—–.–/–.—–.—–.—–.—–.", conveying the message "Mechanics". Furthermore, a Morse code encrypted message of "–.——.—–.–.–/–.———.–.–.–." was successfully transmitted, and the decrypted message was "no pain, no gain" (Figure S32). Similarly, with the six-ligament electrical/thermal dual–responsive 4D printed DPM (160n3–160n4) as the medium, the Morse code "–…—–.—–…–.–/—–.——.–.–…/—.–.—–.—–." was revealed by the selective actuation of the electric field, which was decoded as "metamaterial" (Figure S33).

Due to the highly programmable nature of the 4D printed DPM and the diversity of stimulation methods, the information carrier encryption/decryption procedure was customizable. The encryption/decryption can only be obtained through the pre-set stimulation program, which increased the reliability of information transmission. Furthermore, each pixel was independent, and the metamaterial units comprising i pixel × j pixel were also independent, so that the metamaterial carrier sequence had i × j × n independent pixels. Therefore, metamaterial information carrier sequences were highly independent and flexibly self-assembled, allowing for a high degree of scalability and massive information transfer.

2.4.2. Flexible metamaterial electronics. Flexible robots are emerging in the industrial and medical fields because of their outstanding interactivity and high safety[31, 32]. A key technology of flexible robots lies in the effective and convenient control of flexible structural units, but traditional control units are mostly rigid electronic components, which are difficult to be perfectly compatible with flexible structures. Therefore, based on programmable multi-shape 4D printed gradient metamaterials, variable stiffness logic gate devices were developed to realize the free switching between rigidity and flexibility.

P160n6–T160n3 metamaterials were used as electronic substrates for the logic gates, and adhesive copper foils were used as conductive layers. The P160n6 and T160n3 regions were used as inputs A and B, respectively. Indicator levers were connected at adjacent nodes of the metamaterial to control the on and off state of the circuit. The "AND" logical signal was executed (Figure 8(a)). When the metamaterial P160n6–T160n3 was in its initial shape, the circuit was connected and the LED emitted light ("A = 1, B = 1"). When the metamaterial was programmed into the temporary shape of the straight ligament, the nodes of the cell rotated during this process, causing the indicator levers to deviate from their
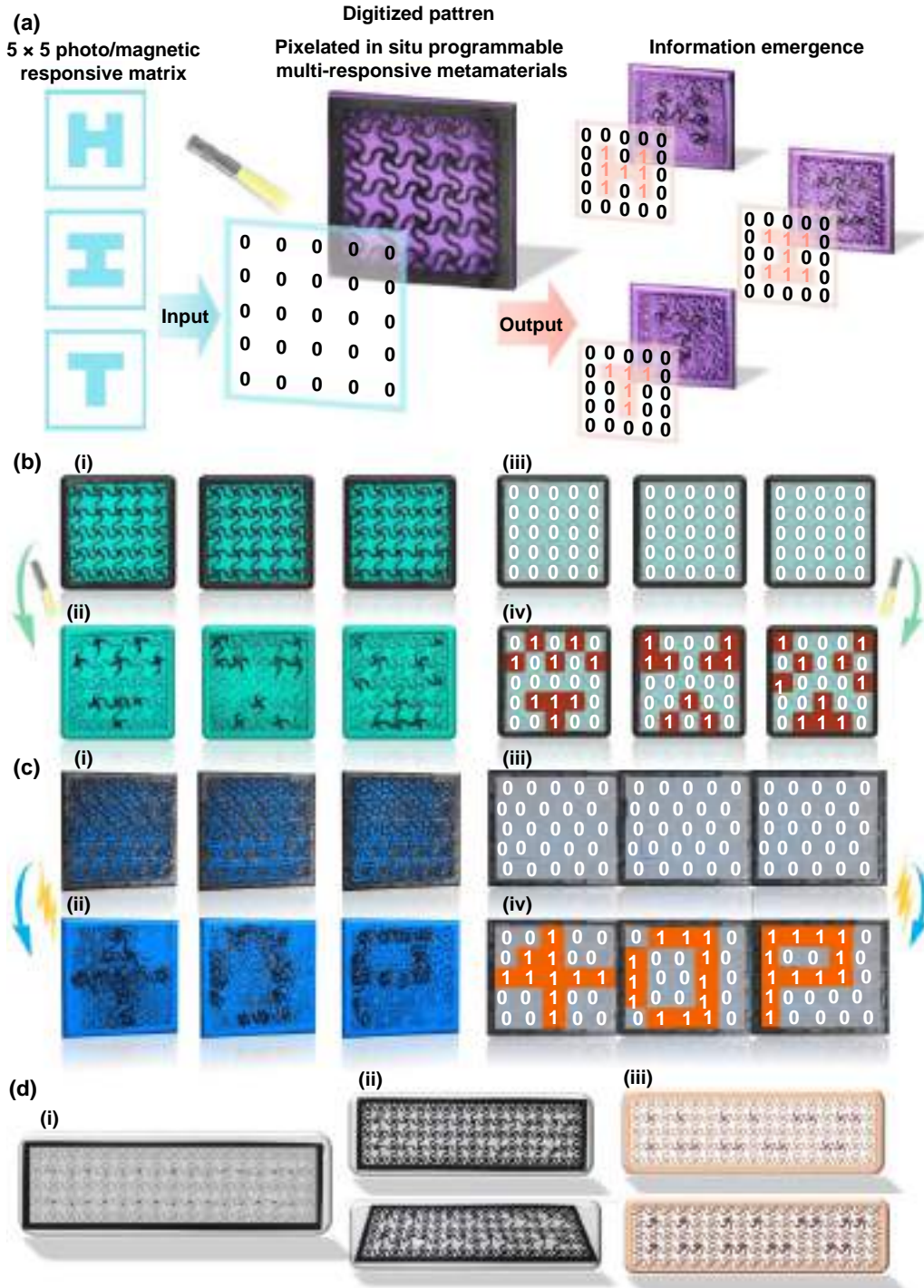
Int. J. Extrem. Manuf. **7** (2025) 055504

Highly programmable 4D printed multi-shape gradient metamaterials...
Yang C et al.

Figure 7. 4D printed DPM intelligent information carriers. (a) The design concept of using binary language "0" and "1" as digital patterns for processing information. (b) and (c) Binary intelligent information carrier. Encrypted information: (b) different expressions, (c) 4DP. (d) Morse Code intelligent information carriers.

original position. Both the end circuits of A and B were disconnected ("A = 0, B = 0"), and the LED light was off. When the metamaterial was exposed to light stimulation, the CNTs absorbed light energy and converted it to thermal energy, and thus the P160n6 region entered a soft rubbery state and underwent shape recovery. The lever at the A end was reset and the logic input was "A = 1, B = 0". When the 4D printed metamaterial was thermally stimulated, the T160n3 region entered

the rubbery state and underwent shape recovery. The B lever was reset and the logic input was "A = 0, B = 1". When the metamaterial completely recovered to its initial shape, both A and B end indicator levers were reset ("A = 1, B = 1") and the LED glowed. Similarly, selective stimulation of 4D printed metamaterials and adjustment of the position of the indicator levers in the circuit can realize the logical operations of OR, XNOR, and XOR (Figures 8(b)–(d)).
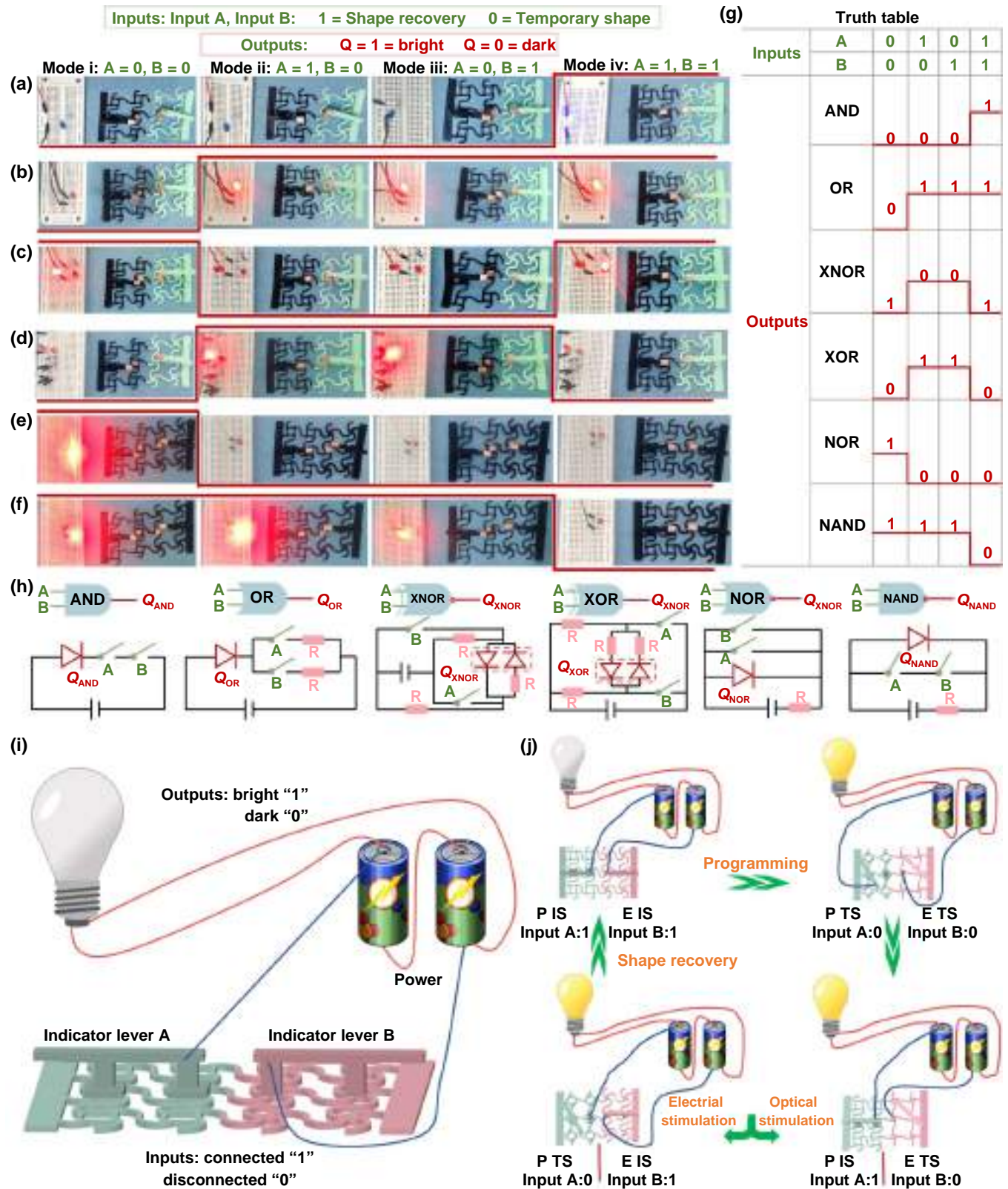
Figure 8. The design of variable stiffness logic electronics based on multi-responsive gradient metamaterials. (a)–(h) The Boolean responses of logic gates in four different configurations (Vertical view): (a) AND, (b) OR, (c) XNOR, (d) XOR, (e) NOR, and (f) NAND logic gate. (g) Truth tables of AND, OR, XNOR, NOR, and NAND logic operations. (h) The schematic diagram of the switching circuit for the logic gates. (i) Schematic diagram of the logic circuit of NAND. (j) The experimental schematic diagram for realizing NAND logic operation based on multi-responsive metamaterial.

Int. J. Extrem. Manuf. **7** (2025) 055504

Highly programmable 4D printed multi-shape gradient metamaterials...
Yang C et al.

Besides, the P160n6–E160n3 (A–B) photo/electrical dual-responsive metamaterial was used as the electronic substrate of the logic gates to realize the logic operations of NOR and NAND (Figures 8(e) and (f)). When the metamaterial was in temporary shape, the indicator levers were disconnected. The logic input was "A = 0, B = 0", while the logical operation result of NOR and NAND was 1, and the LED was illuminated. When the P160n6 region of the metamaterial entered a soft rubbery state under light, the lever at the A end was reset. The logic input was "A = 1, B = 0", where the LED of the NOR gate was off, while that of the NAND gate was on. When the metamaterial was exposed to the electric field, the functional filler CB in the E160n3 region generated Joule heat, and E160n3 was heated into a soft rubbery state. The indicator lever was reset with the deformation of E160n3, corresponding to the input "A = 0, B = 1". The LED of the NOR gate remained off, while the LED of the NAND was on. When both the E160n3 and P160n6 regions returned to their initial shape, the indicator levers at the A and B ends were reset ("A = 1, B = 1"), and the results of the logic operations for both NOR and NAND were 0. The experimental results of each deformation behavior precisely corresponded to the respective truth table of the ideal logical gates (Figure 8(g)), while the schematic diagrams of the serial and parallel switch circuits corresponding to each logic gate are shown in Figure 8(h).

Due to the unique highly programmable characteristics of 4D printed multi-shape metamaterials, combined with multi-stimuli processing, the metamaterial logic gate devices were capable of switching between rigid and flexible states, realizing effective processing of digital signals and precise control of circuits. If different logic units are combined in an orderly manner, the information expression ability and logic judgment ability of variable stiffness logic gates can be further improved to achieve high adaptability and compatibility with flexible robotic systems.

3. Conclusion

In conclusion, multi-responsive SMCs were developed, and multi-shape gradient metamaterials were fabricated in a simple and economically efficient manner by means of multi-material 4D printing technology, manifesting substantial potential for utilization in intelligent information carriers and intelligent flexible robotic system. A systematic analysis of the programmable mechanical properties of 4D printed multi-responsive gradient metamaterials was conducted, revealing the correlation mechanism between the design parameters of ligaments and nodes and the mechanical properties of the metamaterials. By combining binary language and Morse code, programmable digital pixel metamaterials were developed as an intelligent information carrier, achieving high levels of independence, scalability, and personalized design for information encryption and erasure protocols. More intriguingly, variable stiffness logic electronics with free switching between rigid and flexible states were developed

based on the multi-responsive, highly programmable gradient metamaterials, which can effectively process digital signals and precisely control circuits, with the potential to realize an intelligent flexible robot system with integrated sensing-actuation-decision functions.

ORCID iDs

Yanju Liu https://orcid.org/0000-0001-8269-1594
Jinsong Leng https://orcid.org/0000-0003-3594-6528

References

[1] Liu Y, Wang Y Z, Ren H Y, Meng Z Q, Chen X Q, Li Z Y, Wang L W, Chen W, Wang Y F and Du J B. 2024. Ultrastiff metamaterials generated through a multilayer strategy and topology optimization. *Nat. Commun.* **15**, 2984.

[2] Frenzel T, Kadic M and Wegener M. 2017. Three-dimensional mechanical metamaterials with a twist. *Science* **358**, 1072–1074.

[3] Wang D, Dong L and Gu G Y. 2023. 3D printed fractal metamaterials with tunable mechanical properties and shape reconfiguration. *Adv. Funct. Mater.* **33**, 2208849.

[4] Jiao P C, Mueller J, Raney J R, Zheng X Y and Alavi A H. 2023. Mechanical metamaterials and *beyond*. *Nat. Commun.* **14**, 6004.

[5] Alsharif A A, Aviles J M, Zechel F M, Alsharif N A and El-Atab N. 2024. Multi-material direct-ink-writing of silver-based flexible and highly deformable dry electrocardiogram biopatches. *VIEW* **5**, 20240008.

[6] Xu R, Chen C Q, Sun J P, He Y L, Li X, Lu M H and Chen Y F. 2023. The design, manufacture and application of multistable mechanical metamaterials-a state-of-the-art review. *Int. J. Extrem. Manuf.* **5**, 042013.

[7] Choi G P T. 2024. Computational design of art-inspired metamaterials. *Nat. Comput. Sci.* **4**, 549–552.

[8] Jiang S, Liu X J, Liu J P, Ye D, Duan Y Q, Li K, Yin Z P and Huang Y A. 2022. Flexible metamaterial electronics. *Adv. Mater.* **34**, 2200070.

[9] Deng Y, Guo X G, Lin Y S, Huang Z X and Li Y. 2023. Dual-phase inspired soft electronic sensors with programmable and tunable mechanical properties. *ACS Nano* **17**, 6423–6434.

[10] Pan F, Li Y L, Li Z Y, Yang J L, Liu B and Chen Y L. 2019. 3D pixel mechanical metamaterials. *Adv. Mater.* **31**, 1900548.

[11] Zhang M C, Pal A, Zheng Z Q, Gardi G, Yildiz E and Sitti M. 2023. Hydrogel muscles powering reconfigurable micro-metastructures with wide-spectrum programmability. *Nat. Mater.* **22**, 1243–1252.

[12] Zhang X C, Han Y S, Zhu M, Chu Y H, Li W D, Zhang Y P, Zhang Y, Luo J R, Tao R and Qi J F. 2024. Bio-inspired 4D

printed intelligent lattice metamaterials with tunable mechanical property. *Int. J. Mech. Sci.* **272**, 109198.

[13] Zhang Z H, Raymond J E, Lahann J and Pena-Francesch A. 2024. Janus swarm metamaterials for information display, memory, and encryption. *Adv. Mater.* **36**, 2406149.

[14] Choe J K, Yi J, Jang H, Won H, Lee S, Lee H, Jang Y, Song H and Kim J. 2024. Digital mechanical metamaterial: encoding mechanical information with graphical stiffness pattern for adaptive soft machines. *Adv. Mater.* **36**, 2304302.

[15] Fang X, Wen J H, Cheng L, Yu D L, Zhang H J and Gumbsch P. 2022. Programmable gear-based mechanical metamaterials. *Nat. Mater.* **21**, 869–876.

[16] Li S C et al. 2021. Liquid-induced topological transformations of cellular microstructures. *Nature* **592**, 386–391.

[17] Chen J Y, Wang Z F, Yao B W, Geng Y H, Wang C, Xu J H, Chen T, Jing J J and Fu J J. 2024. Ultra-highly stiff and tough shape memory polyurea with unprecedented energy density by precise slight cross-linking. *Adv. Mater.* **36**, 2401178.

[18] Xia Y L, He Y, Zhang F H, Liu Y J and Leng J S. 2021. A review of shape memory polymers and composites: mechanisms, materials, and applications. *Adv. Mater.* **33**, 2000713.

[19] Feng P, Yang F, Jia J Y, Zhang J, Tan W and Shuai C J. 2024. Mechanism and manufacturing of 4D printing: derived and beyond the combination of 3D printing and shape memory material. *Int. J. Extrem Manuf.* **6**, 062011.

[20] Peng B A, Yang Y C, Gu K, Amis E J and Cavicchi K A. 2019. Digital light processing 3D printing of triple shape memory polymer for sequential shape shifting. *ACS Mater. Lett.* **1**, 410–417.

[21] Zhao R Y, Zhao T P, Jiang X Q, Liu X, Shi D, Liu C Y, Yang S and Chen E Q. 2017. Thermoplastic high strain multishape memory polymer: side-chain polynorbornene with columnar liquid crystalline phase. *Adv. Mater.* **29**, 1605908.

[22] Zhang H, Wang D, Wu N N, Li C H, Zhu C Z, Zhao N and Xu J. 2020. Recyclable, self-healing, thermadapt triple-shape memory polymers based on dual dynamic bonds. *ACS Appl. Mater. Interfaces* **12**, 9833–9841.

[23] Lin C, Lv J X, Li Y S, Zhang F H, Li J R, Liu Y J, Liu L W and Leng J S. 2019. 4D-printed biodegradable and remotely controllable shape memory occlusion devices. *Adv. Funct. Mater.* **29**, 1906569.

[24] Qin C and Wu C T. 2022. Inorganic biomaterials-based bioinks for three-dimensional bioprinting of regenerative scaffolds. *VIEW* **3**, 20210018.

[25] Lyu Z Y, Wang J L and Chen Y F. 2023. 4D printing: interdisciplinary integration of smart materials, structural design, and new functionality. *Int. J. Extrem. Manuf.* **5**, 032011.

[26] Jian B C, Li H G, He X N, Wang R, Yang H Y and Ge Q. 2024. Two-photon polymerization-based 4D printing and its applications. *Int. J. Extrem. Manuf.* **6**, 012001.

[27] Cheng W, Zhang J, Liu J and Yu Z Y. 2020. Granular hydrogels for 3D bioprinting applications. *VIEW* **1**, 20200060.

[28] Lin C, Huang Z P, Wang Q L, Zou Z C, Wang W B, Liu L W, Liu Y J and Leng J S. 2023. Mass-producible near-body temperature-triggered 4D printed shape memory biocomposites and their application in biomimetic intestinal stents. *Composites B* **256**, 110623.

[29] Xin X Z, Liu L W, Liu Y J and Leng J S. 2020. 4D printing auxetic metamaterials with tunable, programmable, and reconfigurable mechanical properties. *Adv. Funct. Mater.* **30**, 2004226.

[30] Shen Y, Le X X, Wu Y and Chen T. 2024. Stimulus-responsive polymer materials toward multi-mode and multi-level information anti-counterfeiting: recent advances and future challenges. *Chem. Soc. Rev.* **53**, 606–623.

[31] Mei T, Meng Z Q, Zhao K J and Chen C Q. 2021. A mechanical metamaterial with reprogrammable logical functions. *Nat. Commun.* **12**, 7234.

[32] El Helou C, Buskohl P R, Tabor C E and Harne R L. 2021. Digital logic gates in soft, conductive mechanical metamaterials. *Nat. Commun.* **12**, 1633.